Polímeros
ISSN 1678-5169 (Online)

https://doi.org/10.1590/0104-1428.20250010

ORIGINAL ARTICLES

Analysis of wall-smoothed mesh refinement in polymer melt transient flow

Arthur Henrique Theiss[1] and Diego Alves de Miranda[1]*

[1]Departamento de Engenharia Mecânica, Universidade da Região de Joinville – UNIVILLE, 89288-385, São Bento do Sul, SC, Brasil

**diegoalves_klx@hotmail.com*

Abstract

Several numerical simulation strategies for polymer melt flow have been used to optimize simulation time and reduce numerical errors. It is known that in this type of flow, the emergence of numerical diffusion in the cavity walls is common due to the high stresses caused by highly viscous fluids. In order to avoid uniformly refining the entire mesh and increasing simulation time, a common strategy is to use a localized refinement on the cavity walls. In this context, this study presents a standardization in the smoothing of the mesh on the cavity walls for simulations of transient non-isothermal flow of polymer melts. The main results showed that this type of application is highly efficient and contributes to reducing the time and computational effort of simulations of complex cavities with good accuracy.

Keywords: *injection molds, numerical methodology, molten polymers, smooth mesh refining.*

Data Availability: Research data is available upon request from the corresponding author.

How to cite: Theiss, A. H., & Miranda, D. A. (2025). Analysis of wall-smoothed mesh refinement in polymer melt transient flow. *Polímeros: Ciência e Tecnologia*, *35*(4), e20250046. https://doi.org/10.1590/0104-1428.20250010

1. Introduction

The study of the transient flow of molten polymers is crucial to understanding and optimizing industrial processes, such as extrusion and injection, used in the production of plastic materials[1]. This increase in demand for numerical simulations is due to the fact that through their application it is possible to analyze the behavior of fluids during processes and thus carry out the development of new products and manufacturing improvements without the need for excessive expenses on prototypes or even high demand for project time[2]. Added to the recent technological development and increase in computing capacity, its application has become widespread, having high demand in the current engineering market[3]. However, numerical simulation of these processes presents challenges due to the complexity of the non-Newtonian behavior of polymers and the temporal and spatial scales involved[4]. In this context, mesh refinement is a fundamental step to ensure the accuracy and efficiency of simulations[5]. Mesh quality can significantly affect the stability and convergence of results, especially in transient problems[6].

Numerous experimental and theoretical studies have sought to understand the fundamental aspects behind the rheological responses of polymer melts[7-9]. Guerrier et al.[10] state that numerical simulations are widely applied because they allow tests and analyses to be carried out without the need for test specimens or prototypes, reducing study costs. Herrera and Vieira[11] show that it is crucial to understand the structural and dynamic behaviors of molten polymer molecules in order to manufacture high-quality products. Zhang et al.[12] analyzed adaptive mesh refinement for multiphysics applications through the AMReX software framework, highlighting its possible applications. Sanjaya et al.[13] analyzed the results of simulations with different mesh sizes for wheel rims using the finite element method and compared the accuracy of the results obtained.

Therefore, this study performed the analysis of smoothed mesh refinement in transient polymer melt flow simulations. Innovative and efficient approaches to improve accuracy and reduce computational time are discussed, contributing to significant advances in the modeling and simulation of polymer transformation processes. This study aims to help reduce the computational time spent on simulations and consequently increase the productivity of thermoplastic processing industries. The software used was Ansys Fluent® 2023.R2 and the thermophysical data and rheological properties for verification were taken from the studies carried out by Hétu et al.[14] and Miranda et al.[15].

2. Materials and Methods

2.1 Overview

This study proposes a fully numerical approach to verify the accuracy of smoothed mesh refinement in transient laminar flow of polymer melts. The simulation conditions are shown below.

2.2 Governing equations

The governing equations use the generalized Newtonian formulation (GNF) using Ansys Fluent® 2023.R2, which incorporates the diffusive and convective terms in its original formulation, in addition to resolving these terms in a two-dimensional formulation. Thus, the conservation equations are solved for conservation of mass, momentum and energy, in a fully coupled manner, these differential equations are respectively written as Zdanski and Vaz[16].

$$\frac{\partial \rho}{\partial t}+\frac{\partial(\rho u)}{\partial x}+\frac{\partial(\rho v)}{\partial y}=0 \tag{1}$$

$$\rho\left(\frac{\partial u}{\partial t}+u\frac{\partial u}{\partial x}+v\frac{\partial u}{\partial y}\right)=-\frac{\partial p}{\partial x}+\eta(\dot{\gamma},T)\left(\frac{\partial^2 u}{\partial x^2}+\frac{\partial^2 u}{\partial y^2}\right)+\rho g_x+F \tag{2}$$

$$\rho\left(\frac{\partial v}{\partial t}+u\frac{\partial v}{\partial x}+v\frac{\partial v}{\partial y}\right)=-\frac{\partial p}{\partial y}+\eta(\dot{\gamma},T)\left(\frac{\partial^2 v}{\partial x^2}+\frac{\partial^2 v}{\partial y^2}\right)+\rho g_y+F \tag{3}$$

$$\rho C_p\left(\frac{\partial T}{\partial t}+u\frac{\partial T}{\partial x}+v\frac{\partial T}{\partial y}\right)=k\left(\frac{\partial^2 T}{\partial x^2}+\frac{\partial^2 T}{\partial y^2}\right)+\eta(\dot{\gamma},T)\dot{\gamma}^2 \tag{4}$$

where $\eta(\dot{\gamma},T)$ is the apparent viscosity and the term $\dot{\gamma}$ represents the equivalent deformation rate, which is written as:

$$\dot{\gamma}=\sqrt{2\left(\frac{\partial u}{\partial x}\right)^2+2\left(\frac{\partial v}{\partial y}\right)^2+\left(\frac{\partial u}{\partial y}+\frac{\partial u}{\partial x}\right)^2} \tag{5}$$

The term F is the volume fraction and is determined by the Volume of Fluid (VOF) method.

2.2.1 Volume of fluid (VOF)

The momentum conservation equation is intrinsically associated with the viscosity constitutive relation. The VOF method considers some linear correlations to estimate the viscosity and specific mass at the interface between the molten polymer and the air presented[17]:

$$\rho=\rho_a+(\rho_p-\rho_a)F,\ and\quad \mu=\mu_a+(\mu_p-\mu_a)F \tag{6}$$

In Equations 6, ρ_a and μ_a are the specific mass and dynamic viscosity of the air, while ρ_p and μ_p are the specific mass and dynamic viscosity of the polymer, where $\mu_p=\eta(\dot{\gamma},T)$, is the property that comes from the rheological model. The function of the volume fraction phase F is defined by the following transport equation[17]:

$$\begin{cases} If\ F=1, & for\ a\ point\ inside\ the\ polymer\ domain \\ If\ 0<F<1, & Interface\ between\ the\ phases\ present \\ If\ F=0, & for\ a\ point\ inside\ air\ domain \end{cases} \tag{7}$$

Since the density and dynamic viscosity of the air phase are much lower than those of the same polymer properties, it is assumed that interfacial tension has no relevant effects on the flow. Therefore, in the numerical analysis, the air is replaced by a pseudo-fluid, which has physical properties greater than the real ones.

2.2.2 Polymer rheology

Currently, several rheological models have been developed for applications in simulations of polymers of the most different types of fluid flows. In the study of Miranda et al.[18], several models were tested and compared in relation to obtaining a flow front closer to an experimental result. Based on this study, the authors found that the Modified Cross II (*MC – II*) model yields good results, and for this reason, this rheological model will be chosen to describe the viscosity of the polymer flow during flow. The modified Cross model assumes a pseudoplastic regime and incorporates the temporal relaxation factor of the fluid, being widely applied to model complex systems. The model depends on the deformation rate and temperature, and the equation to be solved is[18]:

$$\eta(\dot{\gamma},T)=\frac{\eta_0(T)}{1+\left[\lambda(T)\dot{\gamma}\right]^{1-n(T)}} \tag{8}$$

$$\eta_0(T)=c_1 e^{\left(\frac{c_2}{T}\right)},\ \lambda(T)=c_3 e^{\left(\frac{c_4}{T}\right)},\ and\quad n(T)=c_5 e^{\left(\frac{c_6}{T}\right)} \tag{9}$$

The polymer chosen for this study was Thermoplastic Olefin (*TPO*), as it has already been used by other authors and obtained all its known thermophysical properties. The rheological properties of *TPO* for *MC – II* are summarized in Table 1[18].

For coupling pressure into the velocity equations in the generalized newtonian fluid (GNF) model, the *PISO* (Pressure-Implicit with Splitting of Operators) method was used[19].

2.3 Boundary conditions

In order to validate the results obtained, the geometry and boundary conditions used by Hétu et al.[14] and Miranda et al.[15] were taken as standard, as represented in Figure 1.

Table 1. Parameters of the viscosity model *MC – II*.

Parameter	Value	Unit
c_1	0.10	Pa • s
c_2	5,277.11	K
c_3	0.001	s
c_4	3,717.262	K
c_5	1.10	K
c_6	653.532	K

The dimensions are respectively $L_0 = 100\,mm$ and $H_0 = 10\,mm$, in addition a flow front in laminar flow and boundary conditions without slip for the cavity walls were defined. The flow front velocity along the geometry can be defined through Equation 10, applied in the validation to ensure an initial condition of the flow front closer to the real one considering the interactions between the fluid and the cavity walls and their respective stresses[20].

$$U_0 = U_i\left(1 - \frac{x^2 + y^2}{\left(H_0/2\right)^2}\right) \tag{10}$$

In its initial condition, the mold cavity is completely filled with air and the initial temperature of the walls, thus all thermophysical properties of the fluids applied in the multiphase validations[18] are represented in Table 2.

2.3.1 Mesh generation

Mesh convergence analysis is extremely fundamental for numerical simulations of transient flow of molten materials[21]. Marin et al.[22] compared the effect of mesh density in the injection pressure, reaching highest precision in a dual-domain mesh with sizes between 2.0 and 4.0 mm. It is worthy to note that the aforementioned mesh sizes are associated with the part or product sizes and shape, especially thickness variations and the presence of free-form shapes. Therefore, one must observe the relative mesh size in order to avoid defining over or under refined meshes.

In some initial tests, it was determined that the mesh size in x would be constant, in which 40 divisions ($\Delta x = L_0 / 40$) proved to be a mesh size with good results. Therefore, the mesh $\Delta x = 2.50\,mm$ was maintained. The Courant number is a local scalar quantity of the fluid domain that represents the advective flow in each control volume.

$$\sigma = |u|\frac{\Delta t}{\Delta x} \tag{11}$$

To maintain the consistency of the transient solutions, considering an initial maximum velocity at the center of the cavity $u = U_i$, a $\Delta t = 0.125\,s$ was initially found. Therefore, all simulations initially have the Courant number $\sigma = 0.50$, which can be considered a value that generates good results for the simulations[15].

To perform the validations of the proposed models, the simulation was applied based on the generation of 5 different types of meshes with an increasing refinement rate Bias Factor (*BF*) in the cells close to the boundary walls, that is, only in y, as shown in Figure 2.

This type of refinement should increase the accuracy of calculations in regions close to the walls of the geometry, avoiding problems such as numerical diffusion. However, the number of nodes and elements will not be changed when applied. Therefore, for all generated meshes, the number of nodes will remain at 861 and the number of elements at 800. The Bias factor, applied to the y –axis and responsible for refining the mesh near the walls of the geometry, doubled for each mesh generated, ranging from 1 to 16, as shown in Table 3.

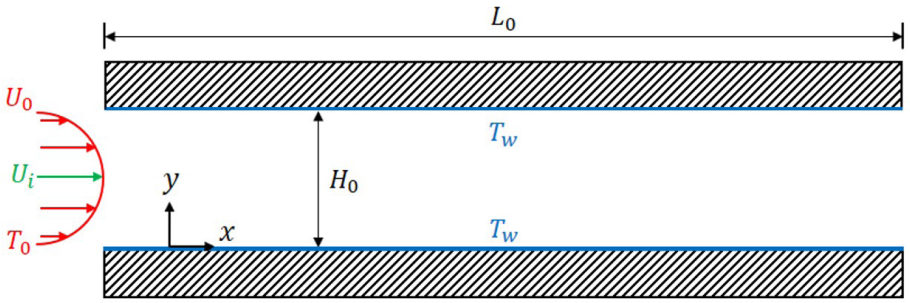

Figure 1. Boundary conditions of 2D fountain flow problem.

Table 2. Thermophysical properties of the fluids used in the validation.

TPO			Air		
Parameter	**Value**	**Unit**	**Parameter**	**Value**	**Unit**
ρ_p	810	$kg \cdot m^{-3}$	ρ_a	1.225	$kg \cdot m^{-3}$
C_{p_p}	2,500	$J \cdot kg^{-1} \cdot K^{-1}$	C_{p_a}	1,006.43	$J \cdot kg^{-1} \cdot K^{-1}$
k_p	0.16	$W \cdot m^{-1} \cdot K^{-1}$	k_a	0.0242	$W \cdot m^{-1} \cdot K^{-1}$
μ_p	$\eta(\dot{y},T)$	$Pa \cdot s$	μ_a	1.7864×10^{-5}	$Pa \bullet s$
U_i	0.01	$m \cdot s^{-1}$	T_a	283	K
T_0	503	K	T_w	283	K

This implies that $BF = h$, ou seja $h_1 = 1.0$, $h_2 = 2.0$, $h_3 = 4.0$, $h_4 = 8.0$ and $h_5 = 16.0$. Richardson[23] estimation requires meshes with equal refinement ratio, where r is the refinement ratio:

$$r = \frac{h_5}{h_4} = \frac{h_4}{h_3} = \frac{h_3}{h_2} = \frac{h_2}{h_1} \quad (12)$$

Thus defining a refinement rate $r = 2.0$ for the Richardson extrapolation method, subsequently applied to measure the degree and order of the discretization error in the calculations performed and evaluate the effect of this refinement on the results obtained. Figure 3 demonstrates the compilation of the generated meshes.

2.4 Dimensionless

In order to qualitatively validate the results obtained in the simulations and after applying the Richardson extrapolation method, the following dimensionless variables were adopted[18]:

$$x^* = \frac{x}{H_0},\ y^* = \frac{y}{H_0},\ t^* = t\frac{U_i}{H_0},\ u^* = \frac{u}{U_i}$$

and

$$T^* = \frac{T - T_w}{T_{0-T_w}} \quad (13)$$

In addition, five lines were plotted along the geometry, from which the values for speed and temperature were generated and analyzed at different time intervals in the validations. Figure 4 represents the geometry and the lines defined for the analysis.

Following the applied dimensionless modeling, the positions of the lines were defined as: $x^* = 1.0$; $x^* = 2.5$; $x^* = 5.0$; $x^* = 7.5$ and $x^* = 10.0$. Furthermore, the time

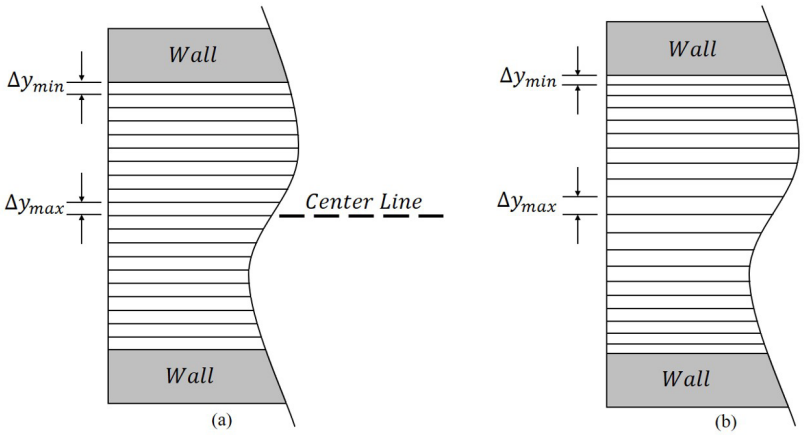

Figure 2. Bias Factor. (a) $BF = 1.0$ ($\Delta y_{max} = \Delta y_{min}$); (b) $BF = 2.0$ ($\Delta y_{max} > \Delta y_{min}$).

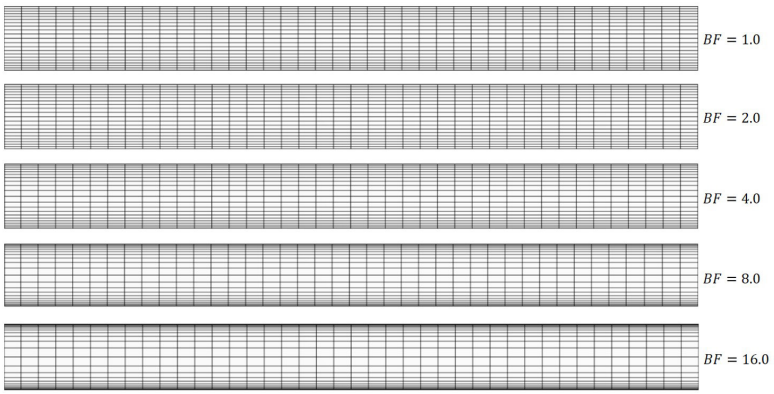

Figure 3. Meshes generated for transient validation.

Table 3. Size of the Meshes Applied in the Simulations.

Size	$BF = 1.0$	$BF = 2.0$	$BF = 4.0$	$BF = 8.0$	$BF = 16.0$
Δy_{min}	0.50 mm	0.362 mm	0.261 mm	0.193 mm	0.152 mm
Δy_{max}	0.50 mm	0.673 mm	0.874 mm	1.10 mm	1.320 mm

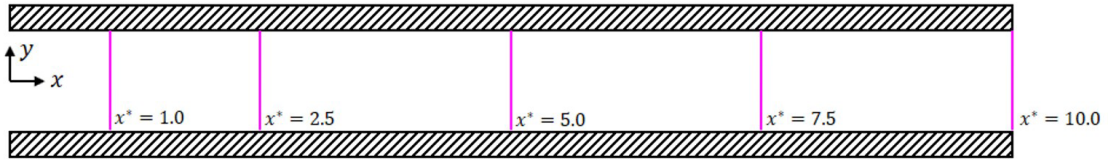

Figure 4. Reference lines.

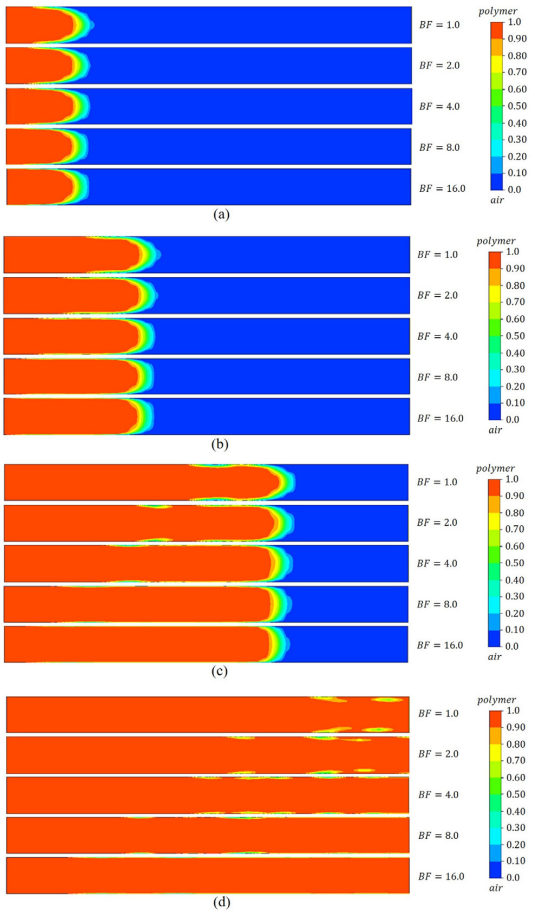

Figure 5. Advance of the flow front during: (a) $t^* = 2.5$; (b) $t^* = 5.0$; (c) $t^* = 10.0$; (d) $t^* = 20.0$.

intervals taken for the analysis of the properties u^* and T^* were $t^* = 2.5$; $t^* = 5.0$; $t^* = 10.0$; and $t^* = 20.$ respectively.

2.5 Convergence analysis

To verify the accuracy of the simulations and the order of the mesh errors in the flow of molten *TPO* in the smoothed mesh discretization channel, the Richardson extrapolation method was implemented[23]. The method assumes that the exact solution for exact velocities and temperatures can be estimated at any given point $x_i \in R^3$ as:

$$\varnothing_{ex}(x_i) = \varnothing_h(x_i) + \varepsilon_h^{\varnothing} = \varnothing_h(x_i) + \alpha h^{p_h} + O\left(h^{p_h+1}\right) \quad (14)$$

$$\varepsilon_{h_1}^{\varnothing} = \varnothing_{ex} - \varnothing_{h_1} \cong \frac{\varnothing_{h_1} - \varnothing_{h_2}}{r^{\tilde{p}} - 1} \quad (15)$$

$$\tilde{p}_{h_1}^{\varnothing} = \frac{\log\left(\dfrac{\varnothing_{h_3} - \varnothing_{h_2}}{\varnothing_{h_2} - \varnothing_{h_1}}\right)}{\log(r)} \quad (16)$$

where $\varnothing$ can represent either u^* or T^*.

3. Results and Discussion

This section will address the results of the numerical approaches applied and their respective discussions.

3.1 Flow analysis

To visually verify the effect of numerical diffusion, the flow through the injection channel of Hétu et al.[14] was simulated in all meshes (Figure 5).

Initially, a qualitative analysis of the results generated by the simulations of different meshes can be made. It can be seen that as the Bias Factor increases, the effects of numerical diffusion reflected on the cavity walls become smaller. These numerical diffusion bubbles become worse as the simulation time increases, i.e., the time variable will increase the numerical error of simulations that obtain coarser meshes.

3.2 Initial values

By applying the Bias Factor it was possible to verify the effects of the smoothed mesh refinement on the accuracy of the results obtained in the simulations. The following Tables 4 to 8 summarize all the results obtained for u^* and T^* throughout the 5 numerical simulations applied.

From the Tables, it is possible to demonstrate that the application of the smoothed mesh refinement throughout the simulations resulted in different values for the same positions and time intervals during the simulated flow. Evidencing that as the mesh refinement rate increased, the precision of the results obtained for the properties under analysis also increased. It is also noted that the relevance of the differences in decimal places obtained in the results is greater for the velocity values when compared with the respective temperatures.

3.3 Verification of transient flow

Based on the previous resulting values, the Richardson error extrapolation method was applied in order to optimize the results obtained. The method was applied for $x^* = 0.01$

Table 4. Velocity and temperature values at $y^* = 0.5$ with $BF = 1.0$.

Time	$x^* = 1.0$		$x^* = 2.5$		$x^* = 5.0$		$x^* = 7.5$		$x^* = 10.0$	
	u^*	T^*	u^*	T^*	u^*	T^*	u^*	T^*	u^*	T^*
$t^* = 2.5$	0.77240	0.97763	–	–	–	–	–	–	–	–
$t^* = 5.0$	0.90119	0.97778	0.77318	0.97769	–	–	–	–	–	–
$t^* = 10.0$	0.90157	0.97778	0.89486	0.97778	0.76940	0.97776	–	–	–	–
$t^* = 20.0$	0.90157	0.97778	0.89487	0.97778	0.89489	0.97767	0.87929	0.97692	0.87637	0.97525

Table 5. Velocity and temperature values at $y^* = 0.5$ with $BF = 2.0$.

Time	$x^* = 1.0$		$x^* = 2.5$		$x^* = 5.0$		$x^* = 7.5$		$x^* = 10.0$	
	u^*	T^*	u^*	T^*	u^*	T^*	u^*	T^*	u^*	T^*
$t^* = 2.5$	0.76159	0.97761	–	–	–	–	–	–	–	–
$t^* = 5.0$	0.89448	0.97777	0.79123	0.97767	–	–	–	–	–	–
$t^* = 10.0$	0.90122	0.97777	0.89240	0.97777	0.84847	0.97773	–	–	–	–
$t^* = 20.0$	0.90125	0.97777	0.89557	0.97777	0.89108	0.97761	0.85918	0.97692	0.88035	0.97525

Table 6. Velocity and temperature values at $y^* = 0.5$ with $BF = 4.0$.

Time	$x^* = 1.0$		$x^* = 2.5$		$x^* = 5.0$		$x^* = 7.5$		$x^* = 10.0$	
	u^*	T^*	u^*	T^*	u^*	T^*	u^*	T^*	u^*	T^*
$t^* = 2.5$	0.75589	0.97760	–	–	–	–	–	–	–	–
$t^* = 5.0$	0.87850	0.97777	0.80032	0.97767	–	–	–	–	–	–
$t^* = 10.0$	0.89989	0.97777	0.85463	0.97777	0.86858	0.97765	–	–	–	–
$t^* = 20.0$	0.89994	0.97777	0.89588	0.97776	0.87208	0.97751	0.85882	0.97677	0.86813	0.97242

Table 7. Velocity and temperature values at $y^* = 0.5$ with $BF = 8.0$.

Time	$x^* = 1.0$		$x^* = 2.5$		$x^* = 5.0$		$x^* = 7.5$		$x^* = 10.0$	
	u^*	T^*	u^*	T^*	u^*	T^*	u^*	T^*	u^*	T^*
$t^* = 2.5$	0.75259	0.97758	–	–	–	–	–	–	–	–
$t^* = 5.0$	0.87814	0.97777	0.79896	0.97766	–	–	–	–	–	–
$t^* = 10.0$	0.89333	0.97777	0.85063	0.97776	0.87207	0.97761	–	–	–	–
$t^* = 20.0$	0.89955	0.97777	0.88940	0.97775	0.87229	0.97734	0.87434	0.97450	0.87666	0.96969

, in which it is possible to obtain values for all defined time intervals ($t^* = 2.5$ to $t^* = 20.0$). Table 9 presents the final results obtained after applying the method:

Thus, after applying extrapolation, it became possible to obtain instantaneous values of greater precision for velocities and temperatures over the defined time intervals. In addition, the degree of error in each of the results obtained was defined. Therefore, it is reiterated that the application of the method allows optimizing the precision of results in numerical approaches without the demand for greater computational capacity and that it proved to be functional for the present study.

From the values obtained in the simulation of the highest refinement rate with $BF = 16.0$ and at e $x^* = 0.5$, the velocity and temperature curves of the exact values were generated and compared with the results obtained by Hétu et al.[14] and Miranda et al.[15] (Figures 6 and 7).

Table 8. Velocity and temperature values at $y^* = 0.5$ with $BF = 16.0$.

Time	$x^* = 1.0$		$x^* = 2.5$		$x^* = 5.0$		$x^* = 7.5$		$x^* = 10.0$	
	u^*	T^*	u^*	T^*	u^*	T^*	u^*	T^*	u^*	T^*
$t^* = 2.5$	0.74822	0.97756	–	–	–	–	–	–	–	–
$t^* = 5.0$	0.87694	0.97777	0.80130	0.97766	–	–	–	–	–	–
$t^* = 10.0$	0.88279	0.97777	0.87361	0.97772	0.87578	0.97750	–	–	–	–
$t^* = 20.0$	0.89954	0.97777	0.87150	0.97772	0.86642	0.97703	0.87874	0.97421	0.88254	0.97039

Table 9. Richardson error extrapolation results for $x^* = 0.01$ and $y^* = 0.5$.

Values	$t^* = 2.5$		$t^* = 5.0$		$t^* = 10.0$		$t^* = 20.0$	
	u^*	T^*	u^*	T^*	u^*	T^*	u^*	T^*
exact	0.75462	0.97773	0.88761	0.97777	0.90465	0.97777	0.90021	0.97777
p_{ave}	0.43604	-0.17229	0.82565	-0.43742	-1.64563	0.00402	1.79979	-0.91733

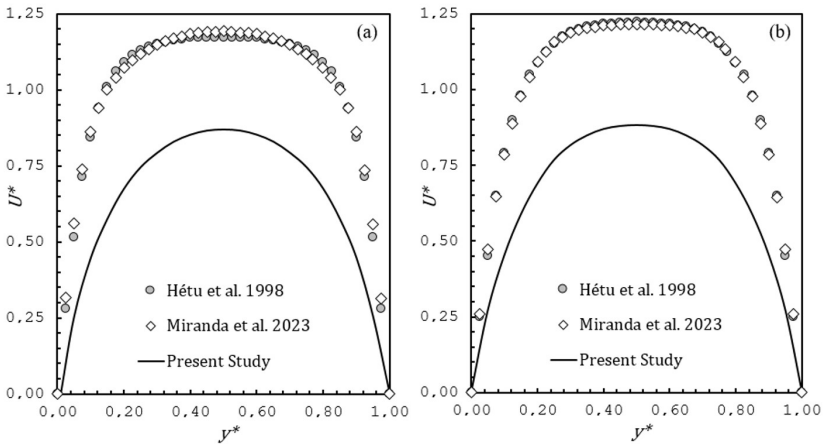

Figure 6. Transient verification of the fountain flow for the velocity profiles at $x^* = 5.0$ to: (a) $t^* = 6.0.$; (b) $t^* = 12.0$.

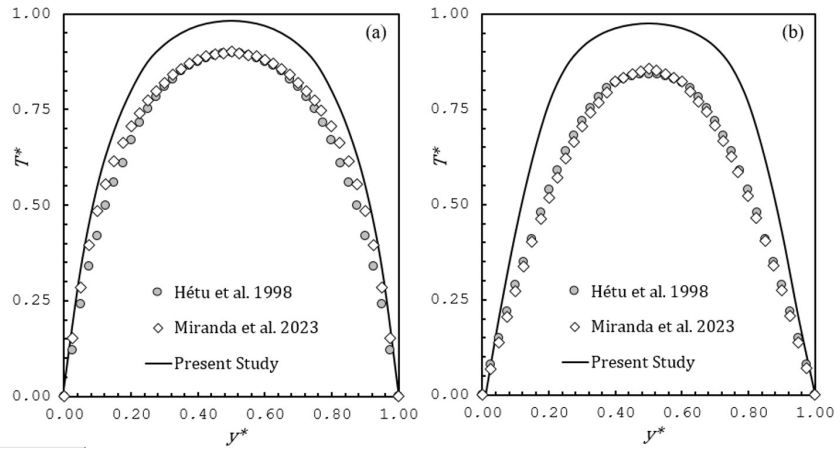

Figure 7. Transient verification of the fountain flow for the temperature profiles at $x^* = 5.0$ to: (a) $t^* = 6.0.$; (b) $t^* = 12.0$.

Analyzing the velocity profiles, there are higher velocity values in the works of Hétu et al.[14] and Miranda et al.[15] because they used a constant velocity at the inlet ($U_0 = U_i$), which causes the polymer to advance faster over time. However, this sudden velocity increase causes the polymer to lose more heat and the temperature profiles to drop consequently, while when the inlet velocity is parabolic, it ends up holding the heat for longer. Although the conditions show very divergent results, in real flow conditions, the polymers usually enter in the gates with a parabolic manner, which confirms that the velocity and temperature curves of this study are more appropriate, and that the verification was successful.

4. Conclusions

Accurate numerical simulations of transient flow of polymer melts are essential to obtain products with desired characteristics, avoiding defects and ensuring process efficiency. This paper presents a numerical approach to smooth mesh refinement in the walls of thermoplastic injection molds and a mesh convergence study using Ansys Fluent® 2023.R2 simulation software. The following points highlight the discussions:

- Initially, the initial velocity equation with parabolic profile proved to be effective in capturing the flow accurately, minimizing the effects of the boundary layer;

- Through the results obtained and validated compared with previous studies, it becomes possible to identify that the application of the smoothed mesh refinement on the walls of the geometry defined for the flow resulted in a significant improvement in the accuracy of the results obtained for the velocity and temperature properties in the applied numerical simulations;

- Furthermore, it was reiterated that through the application of the Richardson error extrapolation method, it was possible to guarantee an improvement in the accuracy of values for certain regions of interest without requiring greater computational resources to obtain them, a fundamental result given the demand for computational resources for simulations in transient regimes;

- Although this study used simple geometry, the qualitative and quantitative results will help engineers reduce the computational time of numerical simulations and consequently increase the productivity of injection mold development with greater efficiency and accuracy.

Furthermore, it is worth highlighting the possibility of future studies using the same method in different types of geometries, such as abrupt expansions, in addition to new analyses for the resulting properties in each of the lines plotted for post-processing of the problem under study and possibly the analysis of other rheological properties of interest.

5. Author's Contribution

- **Conceptualization** – Arthur Henrique Theiss.
- **Data curation** – Arthur Henrique Theiss; Diego Alves de Miranda.
- **Formal analysis** – Arthur Henrique Theiss; Diego Alves de Miranda.
- **Funding acquisition** - NA.
- **Investigation** – Arthur Henrique Theiss; Diego Alves de Miranda.
- **Methodology** – Arthur Henrique Theiss; Diego Alves de Miranda.
- **Project administration** – Diego Alves de Miranda.
- **Resources** – NA.
- **Software** – Arthur Henrique Theiss.
- **Supervision** –Diego Alves de Miranda.
- **Validation** – Arthur Henrique Theiss; Diego Alves de Miranda.
- **Visualization** – Arthur Henrique Theiss; Diego Alves de Miranda.
- **Writing – original draft** – Arthur Henrique Theiss.
- **Writing – review and editing** – Arthur Henrique Theiss; Diego Alves de Miranda.

6. Acknowledgements

The authors gratefully acknowledge CAPES (Coordination for the Improvement of Higher Education Personnel, Brazil) for the financial support.

7. References

1. Zhuang, X., Ouyang, J., Jiang, C., & Liu, Q. (2016). New approach to develop a 3D non-isothermal computational framework for injection molding process based on level set method. *Chinese Journal of Chemical Engineering*, *24*(7), 832-842. https://doi.org/10.1016/j.cjche.2016.04.014.
2. Gruber, P. A., & Miranda, D. A. (2020). Heat transfer simulation for decision making in plastic injection mold design. *Polímeros: Ciência e Tecnologia*, *30*(1), e2020005. https://doi.org/10.1590/0104-1428.08319.
3. Krantz, J., Nieduzak, Z., Kazmer, E., Licata, J., Ferki, O., Gao, P., Sobkowicz, M. J., & Masato, D. (2023). Investigation of pressure-controlled injection molding on the mechanical properties and embodied energy of recycled high-density polyethylene. *Sustainable Materials and Technologies*, *36*, e00651. https://doi.org/10.1016/j.susmat.2023.e00651.
4. Miranda, D. A., Rauber, W. K., Vaz, M., Jr., & Zdanski, P. S. B. (2024). A methodology for determination the inlet velocity in injection molding simulations. *Polímeros: Ciência e Tecnologia*, *34*(1), e20240011. https://doi.org/10.1590/0104-1428.20230099.
5. Marin, F., Souza, A. F., Ahrens, C. H., & Lacalle, L. N. L. (2021). A new hybrid process combining machining and selective laser melting to manufacture an advanced concept of conformal cooling channels for plastic injection molds. *International Journal of Advanced Manufacturing Technology*, *113*(5-6), 1561-1576. https://doi.org/10.1007/s00170-021-06720-4.
6. Perig, A. V., & Golodenko, N. N. (2016). CFD 2D description of local flow of polymer workpiece through a modified U-shaped die during equal channel multiple angular extrusion. *Materials*

Research, *19*(3), 602-610. https://doi.org/10.1590/1980-5373-MR-2016-0013.

7. Zhang, L., Zhao, G., Wang, G., Dong, G., & Wu, H. (2017). Investigation on bubble morphological evolution and plastic part surface quality of microcellular injection molding process based on a multiphase-solid coupled heat transfer model. *International Journal of Heat and Mass Transfer*, *104*, 1246-1258. https://doi.org/10.1016/j.ijheatmasstransfer.2016.09.043.
8. Miranda, D. A., & Nogueira, A. L. (2019). Simulation of an injection process using a CAE tool: assessment of operational conditions and mold design on the process efficiency. *Materials Research*, *22*(2), e20180564. https://doi.org/10.1590/1980-5373-mr-2018-0564.
9. Chen, S.-C., Chien, R.-D., Lin, S.-H., Lin, M.-C., & Chang, J.-A. (2009). Feasibility evaluation of gas-assisted heating for mold surface temperature control during injection molding process. *International Communications in Heat and Mass Transfer*, *36*(8), 806-812. https://doi.org/10.1016/j.icheatmasstransfer.2009.06.007.
10. Guerrier, P., Tosello, G., & Hattel, J. H. (2017). Flow visualization and simulation of the filling process during injection molding. *CIRP Journal of Manufacturing Science and Technology*, *16*, 12-20. https://doi.org/10.1016/j.cirpj.2016.08.002.
11. Herrera, F. Z. F., & Vieira, R. P. (2019). Numerical simulation of atom-transfer radical polymerization of tert-butyl methacrylate. *Materials Research*, *22*(4), e20190333. https://doi.org/10.1590/1980-5373-mr-2019-0333.
12. Zhang, W., Myers, A., Gott, K., Almgren, A., & Bell, J. (2021). AMReX: block-structured adaptive mesh refinement for multiphysics applications. *International Journal of High Performance Computing Applications*, *35*(6), 508-526. https://doi.org/10.1177/10943420211022811.
13. Sanjaya, Y., Prabowo, A. R., Imaduddin, F., & Nordin, N. A. B. (2021). Design and analysis of mesh size subjected to wheel rim convergence using finite element method. *Procedia Structural Integrity*, *33*(1), 51-58. https://doi.org/10.1016/j.prostr.2021.10.008.
14. Hétu, J.-F., Gao, D. M., Garcia-Rejon, A., & Salloum, G. (1998). 3D finite element method for the simulation of the filling stage in injection molding. *Polymer Engineering and Science*, *38*(2), 223-236. https://doi.org/10.1002/pen.10183.
15. Miranda, D. A., Rauber, W. K., Vaz, M., Jr., Alves, M. V. C., Lafratta, F. H., Nogueira, A. L., & Zdanski, P. S. (2023). Analysis of numerical modeling strategies to improve the accuracy of polymer injection molding simulations. *Journal of Non-Newtonian Fluid Mechanics*, *315*, 105033. https://doi.org/10.1016/j.jnnfm.2023.105033.
16. Zdanski, P. S. B., & Vaz, M., Jr. (2006). Polymer melt flow in plane channels: effects of the viscous dissipation and axial heat conduction. *Numerical Heat Transfer Part A*, *49*(2), 159-174. https://doi.org/10.1080/10407780500302059.
17. Tutar, M., & Karakus, A. (2009). Injection molding simulation of a compressible polymer. *Journal of Polymer Engineering*, *29*(6), 355-384. https://doi.org/10.1515/POLYENG.2009.29.6.355.
18. Miranda, D. A., Rauber, W. K., Vaz, M., Jr., Nogueira, A. L., Bom, R. P., & Zdanski, P. S. B. (2023). Evaluation of the predictive capacity of viscosity models in polymer melt filling simulations. *Journal of Materials Engineering and Performance*, *32*(4), 1707-1720. https://doi.org/10.1007/s11665-022-07200-w.
19. Issa, R. I. (1986). Solution of the implicitly discretised fluid flow equations by operatorsplitting. *Journal of Computational Physics*, *62*(1), 40-65. https://doi.org/10.1016/0021-9991(86)90099-9.
20. Mu, Y., Zhao, G., Chen, A., & Wu, X. (2013). Modeling and simulation of polymer melts flow in the extrusion process of plastic profile with metal insert. *International Journal of Advanced Manufacturing Technology*, *67*(1-4), 629-646. https://doi.org/10.1007/s00170-012-4511-7.
21. Rasool, W. I., & Taha, Z. A. (2024). Modelling and numerical simulation during selective laser melting of stainless steel 316L via particle by particle approach. *Materials Research*, *27*, e20230437. https://doi.org/10.1590/1980-5373-mr-2023-0437.
22. Marin, F., Souza, A. F., Pabst, R. G., & Ahrens, C. H. (2019). Influences of the mesh in the CAE simulation for plastic injection molding. *Polímeros: Ciência e Tecnologia*, *29*(3), e2019043. https://doi.org/10.1590/0104-1428.05019.
23. Richardson, L. F. (1911). The approximate arithmetical solution by finite differences of physical problems involving differential equations with an application to the stresses in a masonary dam. *Philosophical Transactions of the Royal Society of London. Series A, Containing Papers of a Mathematical or Physical Character*, *210*(459-470), 307-357. https://doi.org/10.1098/rsta.1911.0009.

Received: Feb. 26, 2025
Revised: Sept. 03, 2025
Accepted: Sept. 16, 2025

Associate Editor: *José A. C. G. Covas*